



Demonstration designs for the remediation of space debris from the International Space Station



Toshikazu Ebisuzaki^{a,*}, Mark N. Quinn^b, Satoshi Wada^a,
 Lech Wiktor Piotrowski^a, Yoshiyuki Takizawa^a, Marco Casolino^{a,c},
 Mario E. Bertaina^{c,d}, Philippe Gorodetzky^e, Etienne Parizot^e,
 Toshiki Tajima^{b,f}, Rémi Soulard^b, Gérard Mourou^b

^a RIKEN, 2-1, Hirosawa, Wako 351-0198, Japan

^b IZEST, Ecole Polytechnique, 91128 Palaiseau, France

^c INFN, Structure of Rome Tor Vergata, Via della Ricerca Scientifica 1, Rome, Italy

^d University of Torino, Via P. Giuria, 1 10125 Torino, Italy

^e APC-CNRS/Paris7 University, 1 rue A. Domonet L. Duquet, 75013 Paris, France

^f Department of Physics and Astron, University of California at Irvine, Irvine, CA 92697, United States

ARTICLE INFO

Article history:

Received 17 December 2014

Received in revised form

3 March 2015

Accepted 4 March 2015

Available online 13 March 2015

Keywords:

Space debris

Laser ablation

International Space Station

ABSTRACT

We present here designs for a staged implementation of an orbiting debris remediation system comprised of a super-wide field-of-view telescope (EUSO) and a novel high efficiency fibre-based laser system (CAN). Initial proof of concept stages will operate from the International Space Station (ISS) where the EUSO telescope has been designed for operation as a detector of ultra-high energy cosmic rays. Equipped with 2.5 m optics and a field of view of $\pm 30^\circ$, the EUSO telescope can also be utilised for the detection of high velocity fragmentation debris in orbit near the ISS. Further tracking, characterisation and remediation are to be performed by a CAN laser system operating in tandem with the EUSO telescope. For full scale versions of both instruments, the range of the detection/removal operation can be as large as 100 km. Utilising a step-by-step approach of increasing scale we present an analysis of implementation of: 1) Proof of principle demonstration of the detection by a mini-EUSO and operation of 100-fibre CAN laser technology as an ISS based prototype, 2) Technical demonstrator of debris-removal that consists of the EUSO telescope for the detection and a 10,000 fibre CAN laser for tracking and impulse delivery for debris re-entry, and 3) A free-flyer mission dedicated to debris remediation in a polar orbit with the altitude near 800 km. The integration of the two novel technologies aboard the ISS amounts to a novel approach as an immediate response to the serious space debris problem with the existing platform of ISS.

© 2015 IAA. Published by Elsevier Ltd. All rights reserved.

1. Introduction

In more than 50 years of spaceflight, over 30,000 t of satellites and rockets have been sent to space. It is estimated that near 3000 t [1] of non-functioning space debris remain in Low Earth Orbit (LEO) in varied forms ranging from fragments to spent rocket bodies and fully intact multi-ton satellites. Since their orbital velocities are very high, collisions can

* Corresponding author. Tel.: +81 48 467 9414.

E-mail address:

ebisu@postman.riken.jp (T. Ebisuzaki).

<http://dx.doi.org/10.1016/j.actaastro.2015.03.004>

0094-5765/© 2015 IAA. Published by Elsevier Ltd. All rights reserved.

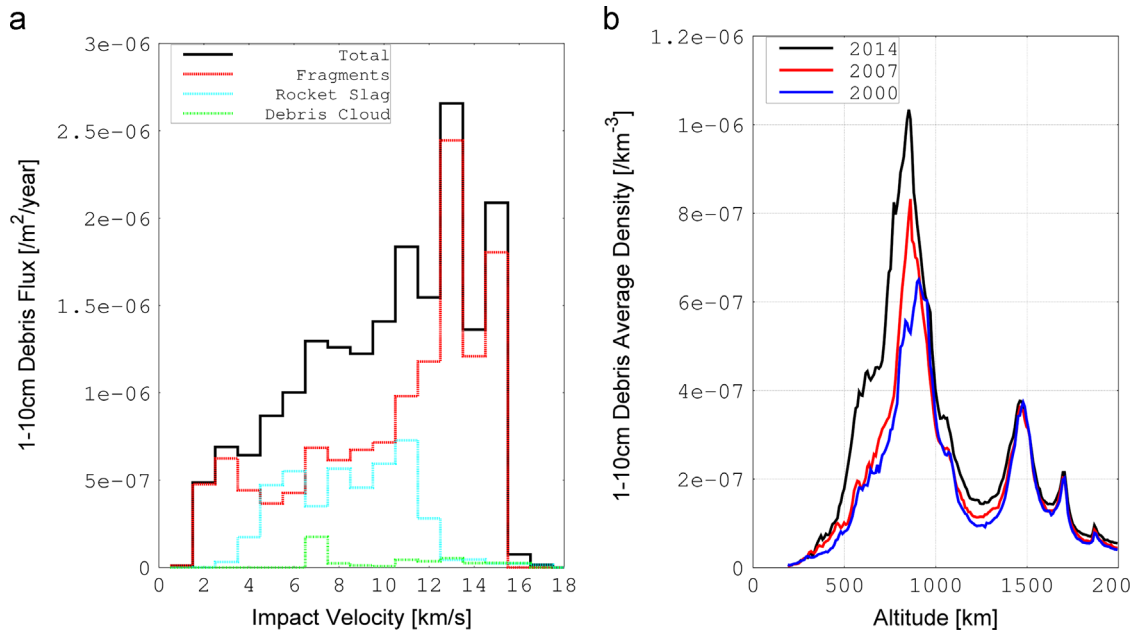


Fig. 1. Results of simulations for 1–10 cm size debris, performed with the MASTER 2009 code [2]: (a) The impact velocity and flux for 1–10 cm debris components calculated for the ISS orbit for 2008, here fragments (red-line) include debris from satellite explosions or collisions. (b) Recent evolution of 1–10 cm debris in low-earth-orbit altitudes. (For interpretation of the references to colour in this figure legend, the reader is referred to the web version of this article.)

involve relative impact velocities of the order of 10 km/s as shown in Fig. 1(a), even the fragments with greater than MJ kinetic energies may cause a severe or catastrophic damage on functioning satellites such as the International Space Station (ISS). In fact, in 1993, the Inter-Agency Space Debris Coordination Committee was established and the discussions concerning control of space debris among space agencies have started.

From a combination of techniques including ground-based radar, surface-impact measurements and statistical modelling the number of debris above 1 cm in size is estimated as $> 7 \times 10^5$. For most spacecraft, including the ISS, debris smaller than 1 cm can be tolerated with adequate shielding. Objects larger than 10 cm can be mitigated using collision avoidance manoeuvres if such debris are first identified and tracked. However, the great majority are not known or catalogued, especially debris with sizes < 10 cm, and hence these hyper-velocity projectiles pose an increasing risk to spacecraft as their population builds. This problem is mounting, since the triggered destruction of a number of satellites in LEO over the last decade including Iridium 33, Cosmos 2251 and Fengyun-1 C. Such large objects are the main source of new debris when hit by numerous smaller fragments in LEO. The small cm-size debris are thus the main threat for impacting the functioning and derelict payloads. The evolution of this population is shown in Fig. 1(b). Much of the increase after 2000 is attributed to the breakup of the aforementioned satellites with significant increases seen for the sun-synchronous polar orbit near 800 km altitude.

Due to their small size and high relative velocity (up to 10 times that of a bullet) there are few viable solutions to remove these projectiles before they collide with larger satellites. The laser impulse control is perhaps such a candidate for

remediation of their orbits. Here pulsed ablation of the debris surface leads to a momentum transfer via the rocket effect. If the orbital velocity is sufficiently reduced, reduction in the altitude of the debris's perigee will enable atmospheric re-entry. With laser pulse thrust of $\ll 1$ N, a rapid train of pulses is required to deliver a total $\Delta v \approx 10^2$ m/s.

Since the late 1980s a number of designs for delivering laser pulses to debris have been proposed operating either from ground-based or space-based. For the latter case, this began with Metzger et al. [3] who proposed a nuclear-powered debris-sweeper with a 10 kJ, 1 Hz krypton fluoride laser (λ of 248 nm). Recently, Phipps [4] proposed a solar-powered space-based system L'ADROIT to be launched consisting of a super-wide-field debris detector with a powerful Nd-Yag laser system with pulse energy of ~ 38 J or more. Schall [5] was the first to propose to use the ISS as a platform for testing debris sweeping technology.

Here in this present paper, we propose to implement a staged approach for evaluating such space based concepts utilising a large wide-field of view detector in tandem with a short pulsed laser beginning with prototypes on-board the ISS as depicted in Fig. 2. At the ISS altitude near 400 km the combined remediation technology can be tested and improved prior to a future design and deployment of freely orbiting systems at higher altitudes such as near 800 km where the debris population in LEO peaks.

Precision determination of debris position and trajectories is a necessity both in the case of avoidance manoeuvres and for attempts at remediation. Here we propose to apply the technology developed for the JEM-EUSO (Extreme Universe Space Observatory on-board Japanese Experiment Module, hereafter EUSO telescope) and designed for the ISS. The JEM-EUSO mission is to detect UV light emitted from the extensive

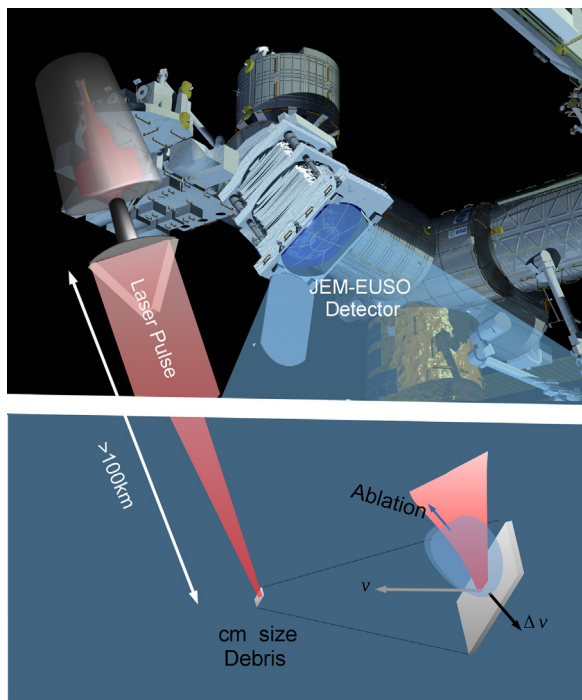


Fig. 2. Concept of our technical demonstrator of the laser removal of debris aboard International Space Station. It consists of the EUSO telescope for acquisition and a CAN laser system for tracking and impulse delivery for cm size debris.

air-showers produced by the ultra-high energy cosmic rays entering the atmosphere at night [7,8]. This detector has a super wide-field of view (FoV) as large as $\pm 30^\circ$ with three double-side Fresnel lenses and a short time resolution down to a few μs with highly pixelized photo-multipliers. During daylight operation, this same detector can provide a unique technology for the detection and position determination of the non-catalogued debris from orbit. Pulsed laser technology has rapidly advanced in the last two decades and it allows us now to consider a space-borne pulsed-laser system. In fact, Soulard et al. [9] proposed to use a space-based laser system applying their Coherent Amplifying Network (CAN) fibre-based technology. A CAN laser is comprised of an array of fibres, each producing a laser beam of ~ 1 mJ, which is phase combined into a beam of total energy of a 1–100 J. Excellent electrical efficiency approaching 30% and a repetition rate higher than 10 kHz are possible which is an ideal solution method for tracking, and impulse delivery to the high velocity debris. Both of these instruments, EUSO and CAN, have been designed for applications in independent physics experiments which are on-going in their development.

This paper is organised as follows. In Section 2, we describe the method of the detection, tracking, and laser impulse control of small debris. In Section 3, a proof-of-principle prototype is described utilising the mini-EUSO telescope which will be installed on the ISS together with a scaled down CAN laser. In Section 4, we present a full scale system designed to test impulse delivery to small space debris from the ISS. In Section 5, we mention a free-flyer mission, dedicated to debris

remediation in a polar orbit with the altitude of near 800 km and evaluation of its performance.

2. Space-based debris remediation

The operation of the space-borne debris remediation system is divided into three stages: 1) passive detection with a super-wide FOV camera, 2) active tracking by a narrow FOV telescope and 3) velocity modification by laser ablation.

2.1. Debris detection

Passive detection of cm-size debris is possible via reflected sunlight in the twilight part of the orbit, where the Earth is in local night and the satellite and the debris are sunlit. In the case of ISS, this corresponds to once about 5 min at every orbit of 90 min (sometimes much more when the ISS path is coincident with the line between day and night). This detection of reflected solar light can be restricted to the U-band (300–400 nm) to avoid the contamination from terrestrial city lights. The flux of photons F_{sun} in the U-band is estimated as $\sim 10^{20}$ photons $\text{m}^{-2} \text{s}^{-1}$ [11]. The photon flux reflected by the debris is calculated as

$$F_{\text{debris}} = \pi d^2 F_{\text{sun}} \xi_E, \quad (1)$$

where ξ_E is the reflection coefficient, and d is the radius of debris, assuming a spherical shape and isotropic scattering at the debris. Using appropriate values for these variables, $\xi_E = 0.1$, $d = 1$ cm, the number of photons scales as

$$F_{\text{debris}} = 3.1 \times 10^{15} \left(\frac{F_{\text{sun}}}{10^{20} \text{ photons m}^{-2} \text{ s}^{-1}} \right) \times \left(\frac{\xi_E}{0.1} \right) \left(\frac{d}{0.01 \text{ m}} \right)^2 \text{ photons s}^{-1}$$

A super wide field-of-view telescope can be used for the detection of the debris by the application of the technology developed for the EUSO mission to detect photons coming from the air-shower produced by ultra-high energy cosmic rays.

The EUSO telescope provides a FoV of $\pm 30^\circ$, an angular resolution of 0.08° , and a time resolution of $2.5 \mu\text{s}$ [10]. The number of photons detected by the telescope is calculated as

$$n_{\text{debris}} = \frac{\zeta D_E^2 F_{\text{debris}}}{16L^2}, \quad (2)$$

where L is the distance to the debris, D_E is the diameter of the optics of the EUSO telescope, and ζ is the collection efficiency of the telescope. A linear track trigger algorithm can be employed for detection of small high velocity debris objects. This algorithm tracks the movement of the debris over a pre-defined time window to distinguish the unique pattern of the track of debris from the background [9].

We set the detection criteria of debris as

$$\text{SNR} = \frac{n_{\text{debris}} \sqrt{T_d}}{\sqrt{B}} \geq 10, \quad (3)$$

where, τ_d is the integration time along the track in the Linear Track Trigger algorithm, and B is the number of background photon flux per pixel [9]

$$B = 4.4 \times 10^5 \left(\frac{\Delta}{0.08^\circ} \right)^2 \left(\frac{\zeta}{0.1} \right) \left(\frac{D_E}{2.5 \text{ m}} \right)^2 \text{ photons s}^{-1} \text{ pixel}^{-1}, \quad (4)$$

where the angular resolution of the EUSO telescope is $\Delta = 0.08^\circ$. Substituting typical numbers for parameters in Eqs. (3) and (4), the minimum detectable debris size by EUSO telescope at 100 km is (Fig. 3)

$$d_{\min} = 7.4 \times 10^{-3} \left(\frac{F_{\text{sun}}}{10^{20} \text{ photons m}^{-2} \text{ s}^{-1}} \right)^{-\frac{1}{2}} \times \left(\frac{\xi_E}{0.1} \right)^{-\frac{1}{2}} \left(\frac{\zeta}{0.1} \right)^{-\frac{1}{4}} \left(\frac{\Delta}{0.08^\circ} \right)^{\frac{1}{2}} \left(\frac{D_E}{2.5 \text{ m}} \right)^{-\frac{1}{2}} \times \left(\frac{L}{100 \text{ km}} \right) \left(\frac{\tau_d}{1 \text{ s}} \right)^{-\frac{1}{4}} \text{ m}, \quad (5)$$

or equivalently the maximum detection distance, $L_{\max, \text{det}}$, for debris size scales (Fig. 4)

$$L_{\max, \text{det}} = 1.4 \times 10^5 \left(\frac{F_{\text{sun}}}{10^{20} \text{ photons m}^{-2} \text{ s}^{-1}} \right)^{\frac{1}{2}} \times \left(\frac{\xi_E}{0.1} \right)^{\frac{1}{2}} \left(\frac{\zeta}{0.1} \right)^{\frac{1}{4}} \left(\frac{\Delta}{0.08^\circ} \right)^{-\frac{1}{2}} \left(\frac{D_E}{2.5 \text{ m}} \right)^{\frac{1}{2}} \times \left(\frac{\tau_d}{1 \text{ s}} \right)^{\frac{1}{4}} \left(\frac{d}{0.01 \text{ m}} \right) \text{ m}. \quad (6)$$

We have to note that τ_d must be considerably shorter than the encounter time, which is about 10 s for the typical case of $L = 100 \text{ km}$ and $v = 10 \text{ km s}^{-1}$. The angular velocity of the debris is also obtained as well. Based on this information, the debris tracking system is evoked, as discussed in the next subsection.

2.2. Debris tracking

The path of the debris has been defined by EUSO with an accuracy of 0.08° linked to the pixel size. Now, we must

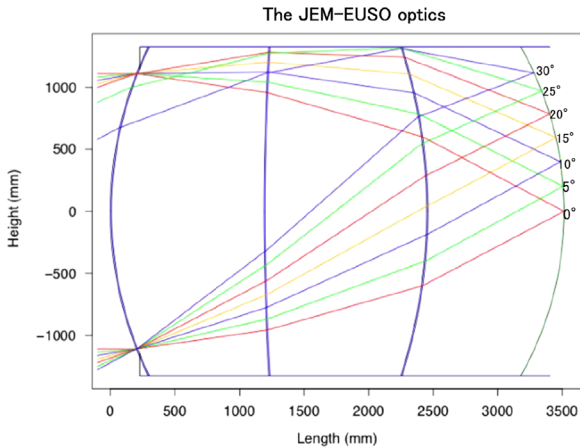


Fig. 3. The cross section and the spot diagram of the JEM-EUSO optics. Two curved and double-side Fresnel lenses and one diffractive Fresnel lens are used to achieve super-wide FoV ($\pm 30^\circ$) [7,8].

track the debris within this 0.08° cone, with an accuracy of the debris size. We call that active debris tracking, which is proposed to employ a combined pulsed laser and a telescope with a FoV consistent with the determination accuracy of the debris detection, which is about the angular resolution of the detection telescope. Thus a series of laser pulses is sent to the debris object where the beam angle is expanded by the telescope to the accuracy of the position determination, described above. The number of laser photons reflected by the debris from N pulses and detected by the telescope can be estimated as

$$n_{\text{laser}} = \left(\frac{NE_p}{hc/\lambda} \right) \left(\frac{\pi d^2}{(\pi \theta L/2)^2} \right) \frac{\xi_T \zeta \pi (D/2)^2}{2\pi L^2} = 3.9 \times 10^4 \left(\frac{\xi_T}{0.1} \right) \left(\frac{\zeta}{0.1} \right) \left(\frac{N}{10^4} \right) \left(\frac{E_p}{10 \text{ J}} \right) \times \left(\frac{d}{0.01 \text{ m}} \right)^2 \left(\frac{D_T}{1.5 \text{ m}} \right)^2 \left(\frac{L}{100 \text{ km}} \right)^{-4} \times \left(\frac{\lambda}{0.35 \text{ } \mu\text{m}} \right) \left(\frac{\Delta}{0.08^\circ} \right)^{-2} \text{ photons}, \quad (7)$$

where E_p is the energy of a laser pulse, ξ_T is the collection efficiency of the tracking telescope, and D_T is the diameter of the tracking optics. The diffraction limited image and the arrival time of the signal enable the three dimensional position of the debris (two position angles and the distance) to be determined.

2.3. Laser ablation of debris

When an intense laser beam is focused on a small area of the debris, its material is ejected as ablation plasma, if the laser intensity is higher than the ablation threshold. Fig. 5 shows the concept of the laser ablation propulsion. For a given energy deposit E , the resultant reaction impact E/v_a is much larger than that of radiation pressure E/c of the laser beam, since the velocity v_a of ablated material is much slower than the light velocity c .

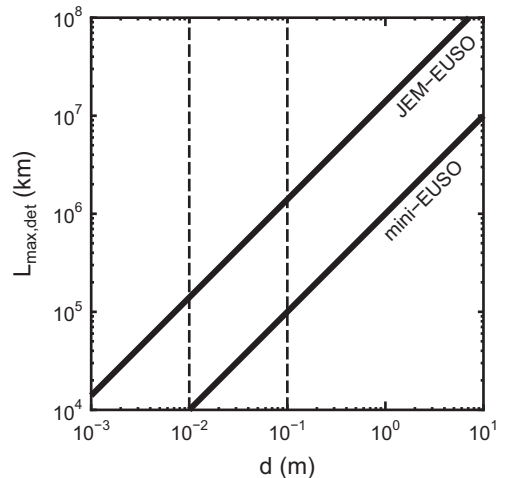


Fig. 4. The actual maximum operation distance $L_{\max, \text{det}}$ is plotted against the debris sized for EUSO ($D_E = 2.5 \text{ m}$, $\Delta = 0.08^\circ$, $\tau_d = 1 \text{ s}$) and mini-EUSO ($D_E = 0.25 \text{ m}$, $\Delta = 0.6^\circ$, $\tau_d = 0.1 \text{ s}$) parameters, where τ_d is the time window necessary to find the debris trajectory.

Space debris, smaller than 10 cm, can be sufficiently decelerated by laser impulses resulting in its re-entry to the Earth's atmosphere, as shown in Fig. 6. Here the debris of mass m are transferred to a lower orbit via a deceleration of Δv . The total laser energy required can be estimated as, $E_L \approx m C_m \Delta v$ where C_m is the efficiency of coupling to debris. For a given laser pulse duration and debris material, the optimal C_m requires a specific fluence to be delivered onto debris surface [6]. Fig. 6 shows the scheme of the shooting operation. Here EUSO telescope and the tracking optics are tilted backward 25° from the nadir, where the relative velocities of the debris are as low as 2 km s⁻¹ (see Figs. 7 and 8).

Focusing of the pulse energy to the necessary fluence at large distances is limited by diffraction to radius

$$b = \frac{a M^2 \lambda L}{D} = 2.0 \times 10^{-2} \left(\frac{a}{0.85} \right) \left(\frac{\lambda}{0.35 \mu\text{m}} \right) \left(\frac{M^2}{1.0} \right) \times \left(\frac{D}{1.5 \text{ m}} \right)^{-1} \left(\frac{L}{100 \text{ km}} \right) m, \quad (8)$$

which is dependent on the quality of the laser beam (M^2) with aperture D , wavelength λ and the L . In addition, the beam profile also limits the minimum focal spot by factor a , which equals 1.27 for a classic airy pattern. According to Phipps et al. [12], the coupling coefficient C_m takes around 10^{-4} N/W for in the pulse duration τ_p shorter than 1 ns, if the fluence $F \sim 10^4$ J m⁻². In other words, the condition for the laser ablation is expressed as

$$F = \frac{E_p}{\pi(b/2)^2} \geq F_{\text{th}} = 10^4 \text{ J m}^{-2}$$

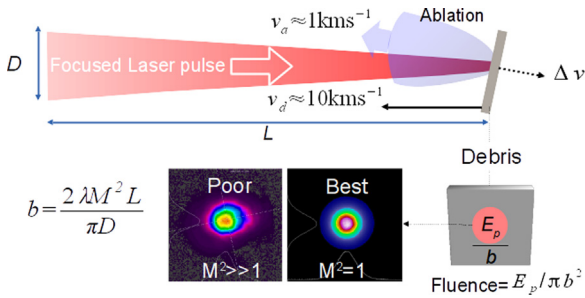


Fig. 5. Concept of the propulsion by laser ablation. Ablated material is ejected as ablation plasma by the velocity of v_a .

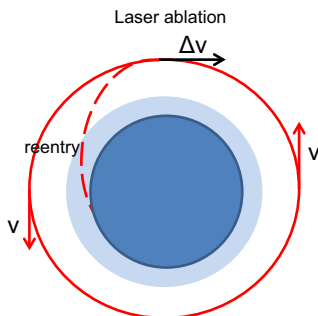


Fig. 6. The concept of the removal of debris by laser ablation. Reducing the speed of debris by Δv via laser-ablation impulses.

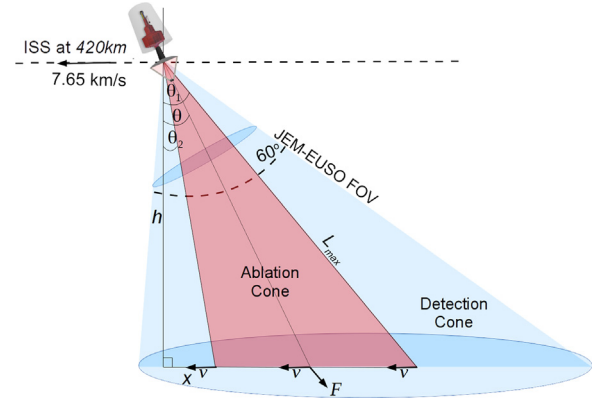


Fig. 7. The scheme of the shooting operation from ISS. The detection telescope and tracking optics are co aligned and tilted backward by 25° from the nadir. The shooting takes place from $\theta_1 \sim 40^\circ$ to $\theta_2 \sim 10^\circ$.

The maximum ablation distance $L_{\text{max, ab}}$ is determined as

$$L_{\text{max, ab}} = \frac{2D}{a M^2 \lambda} \left(\frac{E_p}{\pi F_{\text{th}}} \right)^{1/2} = 1.5 \times 10^5 \left(\frac{a}{0.85} \right)^{-1} \left(\frac{M^2}{1.0} \right)^{-1} \left(\frac{\lambda}{0.35 \mu\text{m}} \right)^{-1} \times \left(\frac{D}{1.5 \text{ m}} \right) \left(\frac{E_p}{10 \text{ J}} \right)^{1/2} \left(\frac{F_{\text{th}}}{10^4 \text{ J m}^{-2}} \right)^{-1/2} m. \quad (9)$$

The laser energy deposited E_d on to the spherical debris with radius d by one pulse is calculated as

$$E_d = 1.0 \times 10^1 \left(\frac{E_p}{10 \text{ J}} \right) \min \left(1, \left(\frac{d}{b} \right)^2 \right) \text{ J}. \quad (10)$$

The average laser reaction force f_L exerted on the debris is calculated as

$$f_L = C_m E_d R = 1.0 \times 10^1 \left(\frac{C_m}{10^{-4} \text{ N/W}} \right) \left(\frac{E_d}{10 \text{ J}} \right) \left(\frac{R}{10^4 \text{ Hz}} \right) \text{ N}, \quad (11)$$

The time integrated force (impact) I by a laser operation along the direction of the motion of the debris

$$I = -\frac{h}{v} \int_{\theta_1}^{\theta_2} \frac{f_L d\theta}{\cos \theta} = \gamma I_0, \quad (12)$$

where $I_0 = C_m E_d R h / 2v$, and θ is the angle between the directions of force and the debris motion, h the impact parameter of the debris and γ the parameter of the order of unity for most of cases and represented by

$$\gamma = \int_{\theta_1}^{\theta_2} \frac{\min \left(1, \left(\frac{d}{b} \right)^2 \right) d\theta}{\cos \theta} = \left(\frac{Dd}{a M^2 \lambda h} \right)^2 \times (\sin \theta_2 - \sin \theta_1) \quad \text{for } d < \frac{a M^2 \lambda h}{D \cos \theta_2}$$

$$= \ln \frac{1 + \sin \theta_0}{1 - \sin \theta_0} - \ln \frac{1 + \sin \theta_2}{1 - \sin \theta_2} + \left(\frac{Dd}{a M^2 \lambda h} \right)^2 \times (\sin \theta_1 - \sin \theta_0) \quad \text{for } \frac{a M^2 \lambda h}{D \cos \theta_2} < d < \frac{a M^2 \lambda h}{D \cos \theta_1}$$

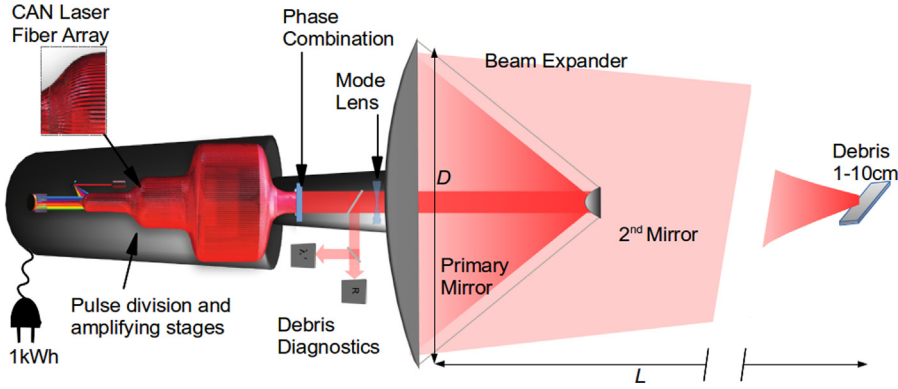


Fig. 8. The CAN concept for the debris removal module. Powered by stored solar energy from the parent satellite, the amplified beam from the combined array of fibres is expanded via the telescope to aperture D which enables focusing to large distances, $L \sim 100$ km, while the phase array controls the wavefront and hence the focal distance of the beam.

$$= \ln \frac{1 + \sin \theta_1}{1 - \sin \theta_1} - \ln \frac{1 + \sin \theta_2}{1 - \sin \theta_2} \quad \text{for } d > \frac{aM^2 \lambda h}{D \cos \theta_1}, \quad (13)$$

where the orbit of debris is assumed by a horizontal straight line, $\theta_0 = \cos^{-1}(aM^2 \lambda h / Dd)$ and θ_1 and θ_2 the angles at which shooting starts and ends, respectively. The velocity change Δv by an impact/

$$\begin{aligned} \Delta v &= 3.0 \times 10^1 \left(\frac{\gamma}{1.0} \right) \left(\frac{C_m}{10^{-4} \text{ NW}^{-1}} \right) \left(\frac{E_p}{10 \text{ J}} \right) \left(\frac{R}{10^4 \text{ Hz}} \right) \\ &\times \left(\frac{h}{100 \text{ km}} \right) \left(\frac{v}{2 \text{ km s}^{-1}} \right)^{-1} \left(\frac{\rho}{2 \times 10^3 \text{ kg m}^{-3}} \right)^{-1} \\ &\times \left(\frac{d}{0.1 \text{ m}} \right)^{-3} \text{ m s}^{-1}, \quad (14) \end{aligned}$$

For the case of debris in the LEO. The reduction Δr in the orbital radius of debris by an instantaneous change in the orbital velocity is given by [5]

$$\begin{aligned} \Delta r &= 1.0 \times 10^2 \left(\frac{\Delta v}{30 \text{ m s}^{-1}} \right) \text{ km} \\ &= 1.0 \times 10^2 \left(\frac{\gamma}{1.0} \right) \left(\frac{C_m}{10^{-4} \text{ NW}^{-1}} \right) \left(\frac{E_p}{10 \text{ J}} \right) \\ &\times \left(\frac{R}{10^4 \text{ Hz}} \right) \left(\frac{h}{100 \text{ km}} \right) \left(\frac{v}{2 \text{ km s}^{-1}} \right)^{-1} \\ &\times \left(\frac{\rho}{2 \times 10^3 \text{ kg m}^{-3}} \right)^{-1} \left(\frac{d}{0.1 \text{ m}} \right)^{-3} \text{ km}. \quad (15) \end{aligned}$$

The minimum operation distance L_{\min} is determined by the maximum speed of the tracking system, which is likely to be less than 10 degrees $^{-1}$, so that

$$L_{\min} = 1.1 \times 10^1 \left(\frac{v}{2 \text{ km s}^{-1}} \right) \left(\frac{\omega}{10 \text{ degrees}^{-1}} \right)^{-1} \text{ km}, \quad (16)$$

where ω is the angular velocity of the debris. The cross section A_{sh} of the shooting area is estimated as

$$\begin{aligned} A_{\text{sh}} &\sim h^2 \tan \varphi_1 = L_{\max}^2 \cos^2 \theta_1 \tan \varphi_1 = 1.6 \\ &\times 10^9 \left(\frac{L_{\max}}{100 \text{ km}} \right)^2 \text{ m}^2 \quad (17) \end{aligned}$$

For $\theta_1 = 40^\circ$, $\varphi_1 = 15^\circ$, and $L_{\max} = \min(L_{\max, \text{ab}}, L_{\max, \text{det}})$.

It should be noted that these calculations do not consider the effects of debris spin or its orientation with respect to the laser pulse direction [6]. However, with high repetition laser pulses, i.e. $> \text{kHz}$, it can be possible to rapidly probe the orientation and angular velocity of the debris without modifying its trajectory. Ablation should thus be carried out only once such debris characteristics are known to ensure impulse delivery is optimised for remediation.

3. The CAN laser system

In choosing a laser system for active tracking and de-orbiting of small debris, there are a number of design factors which should be considered for operation on-board the ISS. Primarily the limited provision of solar power necessitates a laser system with high electrical efficiency. Likewise, with very high relative velocities > 10 km/s between laser source and debris, interaction times are short (< 10 s), and hence a fast response and good average power are demanded. Heat dissipation, compactness and robustness are also key factors for operation in space. Many of these factors are absent with traditional gas or crystal-based laser technology which are limited by poor wall-plug efficiency $< 0.1\%$ and poor heat dissipation restricting the repetition to a few pulses per second and hence providing very low average power (~ 10 W). However, with the rapid development of fibre-based diode-pumped laser science, embodied by the CAN concept, these design factors can be realized.

The original concept for a CAN laser by Mourou et al. [13] involved propagating a seed laser pulse through a network of mono-mode fibres and multiple stages of dividing and amplification. At the end of the network, there are $N \gg 10^3$ pulses which are then coherently combined both in time and phase to produce an overall array of laser pixels. Each channel in the array provides 1 mJ of laser energy with efficient diode-pumping, with total energy of $N \times 1$ mJ per pulse, $\lambda = 1 \mu\text{m}$ wavelength and pulse duration of ~ 100 ps. With individual phase control of each pixel, the resulting beam can be of excellent spatial quality. A very high degree of beam control is possible providing diffraction limited focusing and beam shaping with the potential for adapting heuristically to target surface interaction. Development of this new laser

architecture is ongoing with the international or ICAN consortium, recent progress has demonstrated coherent combination with phase error $\lambda/60$ rms using 64 fibres in continuous wave mode [14]. Pulsed operation has been demonstrated for 4 fs channels totalling 1.3 mJ and with over 90% combining efficiency [15]. Beam steering is enabled with such phase control and is limited to the beam separation (d) as $\lambda/d \approx 1$ mrad, although much larger values have been measured by Bourderionnet et al. using a translatable lens array [16]. Scalability is inherent in this network approach, with arrays of 1000 and 10,000 fibres planned for prototype demonstrations.

By virtue of their intrinsic geometry, the surface area of optical fibres enable more effective dissipation of heat than traditional media providing access to kHz repetition rates in pulsed-mode. Similarly, the orders of magnitude improvement in electrical efficiency of diode pumping over traditional lasing-media is well known ($> 30\%$) as is their high average power (> 10 kW). Transport within single mode fibres provides increased robustness of the system which is critical for stability of optical systems in orbit.

A conceptual design for the CAN debris interaction module is shown in Fig. 8. Here, stored solar energy from the ISS provides the power required for the multi-channel fibre laser. In order to deliver pulses over ~ 100 km, the beam would be expanded to metre scales via multiple optics such as a simple telescope design. Here primary and secondary mirrors provide mechanical motion to steer and focus the beam with coarse precision over a FoV of 10° . With the inclusion of beam expanding optics we expect that phase control enables precision steering of 0.05 mrad with a precision of 0.01 μ rad. Similarly, focusing is finely controlled from a broad beam to a diffraction limited spot on the target when sufficient fluence is required to induce ablation and recoil impulses. Since phase adjustment can occur at rates of $\sim 10^3$ Hz, debris surface condition scan be evaluated with trains of pulses and to tailor the beam profile for an optimal interaction. Such a heuristic approach could rapidly scan and optimise the coupling in terms of recoil thrust or reflectivity with debris of distinct orientation, rotation and surface type.

As reported in Soulard et al. [9], a configuration of 10^4 fibres results in a pulse energy of 10 J, an ablation range with best focus of 20–60 km for $D_T = 1.5$ m beam aperture. We can evaluate the performance of this system if it is employed in a nadir configuration on-board the ISS with the EUSO instrument. If operating at high rep-rate (10 kHz) the laser could deliver very high average powers ~ 100 kW. Since rates of debris of $\ll 1$ /hr are expected, a MJ of laser energy for debris ablation could be stored as 0.3 kWh which, including efficiency losses, would be ~ 1 kWh equivalent to 8 kg of Li-ion batteries, assuming a power density of 130 Wh/kg.

A key challenge is the rapid beam pointing required when engaging debris, since the angular velocity of a debris is as high as 0.1 rad/s for the typical case of 10 km s^{-1} relative velocity and 100 km distance. Such a high speed requires special consideration in the mechanical design of the expanding optics. If necessary, we can only engage debris with the relative velocity less than 10 km s^{-1} , and may remove them in further encounters with more favourable conditions.

4. Proof of principle and prototype systems on-board the ISS

In using the combined technology for the EUSO and CAN systems we propose a development in two steps on-board the ISS before realising a remediation system

1. Scaled down proof of principle design operating from the ISS.
2. Technical demonstrator capable of testing debris remediation operating from the ISS.
3. Free orbiting system to remove most of LEO debris near 800 km.

A summary of the specification of these systems is shown in Table 1. Further details are discussed in the following section.

4.1. Proof of principle system with mini-EUSO

The prototype system will be installed on-board the ISS to demonstrate the technical feasibility of our concept in an LEO environment. Here the detection of debris can be performed by the mini-EUSO system which is the prototype of the EUSO instrument. Its primary mission to observe the atmospheric cosmic ray events will be restricted to dark sky conditions resulting in a $\approx 20\%$ duty cycle. Some 20% of the remaining mission time is suitable for debris detection during which the ISS is in twilight while the debris are in sunlight. The Italian space Agency has approved to launch in the framework of the VUS-2 (Human Space Flight 2) call, with the flight scheduled tentatively in 2016.

Mini-EUSO is a super wide field camera with two Fresnel lens (0.25 m in diameter) and a Multi-Anode-Photo-Multiplier-Tube (MAPMT) array as the focal surface detector. As shown in Fig. 8, the diameter of the Mini-EUSO optics is 0.25 m, the angular resolution is 0.8 degree (0.014 rad), Field of View of $\pm 18^\circ$ and a time resolution of 2.5 μ s. This signal is one order of magnitude higher than background photons, which is as low as one photon per GTU (2.5 μ s). The integration time of 1 ms is more than enough collect photons to calculate position and the orbit of the debris. Since the angular velocity of a debris fragment at the distance of 1 km is typically 1° ms^{-1} , mini-EUSO can track the debris with a large margin.

The maximum detection distance of mini-EUSO is about 100 km for debris size of 0.1 m (see Fig. 3), the cross section of the detection area is estimated as $L_{\max}^2 \sin \varphi_1 \sim 3.1 \times 10^9$ m² for $L_{\max} = 10^5$ m, $\varphi_1 = 18^\circ$, and $d > 0.1$ m. As the debris flux is about 1×10^{-7} m⁻² yr⁻¹ for > 0.1 cm, approximately 310 debris should pass the ISS within a distance of 100 km. It is therefore expected to detect 15–30 debris per year assuming that the mini-EUSO is restricted to ISS twilights, which takes place 5 min every 90 min.

After the detection, we will conduct the experiment to irradiate the detected debris using a prototype low power ICAN laser system made with 100 fibres. The successful irradiation can be confirmed by the brightening of the debris by the reflected laser photons. The number of laser photons of the wavelength of 350 nm reflected by debris is

Table 1

Design parameters for testing debris remediation systems. Evolving initially onboard the ISS, the 'Prototype' provides testing of the key technologies in space and their operation in tandem, to be followed by a scaled-up 'Demonstrator' system to realise large distance delivery of pulses with sufficient fluence for Δv and directed propulsion. Once these systems have been proven reliable on the ISS, a free orbiting 'Dedicated' system can be considered for other more debris critical orbits such as near 800 km. For the latter 2 systems, laser focusing should be to the scale of the debris size at 100 km, with beam quality $M^2=1$ and delivered pulse fluence $\sim 10^4 \text{ Jm}^{-2}$.

	Prototype at ISS orbit (400 km)	Demonstrator at ISS orbit (400 km)	Dedicated system near 800 km
Debris size (cm)	> 1	$10 > d > 0.5$	$10 > d > 0.5$
Debris distance (km)	~ 100	~ 100	~ 100
Detector aperture	0.25 m	2.5 m	2.5 m
Photon detector (detection)	MAPMT	MAPMT	MAPMT
Wavelength (nm)	350–400	350–400	350–400
Angular resolution ($^\circ$)	0.8	0.08	0.08
Time resolution (μs)	2.5	2.5	2.5
Field of view	$\pm 14^\circ$	$\pm 30^\circ$	$\pm 30^\circ$
Background (photons/ms)	300	300	300
Pixel crossing time (ms)	10	1.2	1.2
S/\sqrt{N} ratio	600	60	60
Laser focusing optics	0.25 m	1.5 m	1.5 m
Laser wavelength (nm)	335	355	355
Photon detector (tracking)	SiPM	SiPM	SiPM
Field of view ($^\circ$)	1.2	0.6	0.6
Spatial resolution (μrad)	10	0.3	0.3
Number of pixels	200×200	1600×1600	1600×1600
Response time (s)	0.01	3	3
Time resolution (ns)	1	1	1
Pulse energy (J)	0.1	1	1
Laser system	10^2 Fibres	10^4 Fibres	10^4 Fibres
Pulse energy (J)	0.1	10	10
Pulse duration (ns)	1	0.1	0.1
Repetition rate (Hz)	10^2	10^4	5×10^4
Laser average power (W)	10	10^5	5×10^5
Events per year	20–30 (detection)	10 (backward)	1.6×10^5 (forward)
	2–3 irradiation)	300 (forward)	1.6×10^3 (backward)

estimated as

$$\begin{aligned}
 n_{\text{laser}} &= \frac{\xi \zeta E_p N d^2 D^2}{(hc/\lambda) \theta^2 L^4} = 1.0 \\
 &\times 10^1 \left(\frac{\xi}{0.1}\right) \left(\frac{\zeta}{0.1}\right) \left(\frac{N}{10^2}\right) \left(\frac{E_p}{0.1 \text{ J}}\right) \left(\frac{\lambda}{0.35 \mu\text{m}}\right) \\
 &\times \left(\frac{d}{0.03 \text{ m}}\right)^2 \left(\frac{\theta}{0.01 \text{ rad}}\right)^{-2} \left(\frac{L}{10 \text{ km}}\right)^{-4} \\
 &\times \left(\frac{D}{0.25 \text{ m}}\right)^2 \text{ photons,} \quad (18)
 \end{aligned}$$

where θ is the opening angle of the beam.

By this experiment with prototype EUSO and ICAN systems, we establish the technology to irradiate the debris by a laser beam immediately after the detection by a large angle detector. In the next step, we increase the diameter, field of view of the detector and laser power, where the steering accuracy of the latter is sufficient for debris de-orbiting, as we will discuss in the next subsection.

4.2. Technical demonstrator of laser removal with EUSO

A technical demonstrator of a debris removal system is composed of a 2.5 m EUSO telescope for the detection and a scaled up CAN laser with a larger mirror. Continuing from the prototype experiment, this combined system will be housed on the International Space Station. The goal now will be to

demonstrate detection, tracking and complete removal of 5 mm to 10 cm debris fragments from this orbit.

The EUSO optics consists of two curved double-sided Fresnel lenses with a diffractive Fresnel lens in between for chromatic aberration reduction. The combination of three Fresnel lenses achieves a full angle FoV of 60° . As with its prototype, mini-EUSO, the EUSO telescope has been designed for cosmic ray observation on-board the ISS [7,8]. This module can operate in the nadir direction (planned for the first two years) or in a tilted configuration up to an angle of 30° relative to nadir (for the rest of its mission) during the night. In terms of debris detection, it can be operated during the period of astronomical twilight or day time. Twilight operation is the best opportunity to detect debris since the sun still illuminates the objects in the ISS orbit in contrast to the dark background, where the sunlight cannot illuminate. The EUSO telescope can also detect debris in day time if it is directed above the horizon where the background photons flux is expected to be much lower than the surface of the Earth. The operation of the EUSO mission must be carefully redesigned to include the debris removal operation to compromise different tasks.

The CAN laser module will include a 1.5 m Cassegrain telescope. This will entail a dual function: as a beam expander to enable longer focal distances and as a collector of reflected photons which will be imaged to provide diagnostic data on the debris. The detector here will comprise silicon

photomultiplier (SiPM) technology with 4800×4800 pixels of 1 mm size with a time resolution of 1 ns. The number of background photons in 1 ns is negligible compared with the number of signal photons reflected by the laser as estimated in equation 24. As for the laser system, a 10,000 fibre system will be capable of producing an average power of 100 kW (Table 1), as described in Soulard et al. [9].

In order to estimate the effectiveness of this combined system for debris remediation we can calculate the expected debris flux for 5 mm to 10 cm fragments. Results obtained with MASTER-2009 are shown in Fig. 10. Here the orbit is that of the ISS and debris distributions are of 2014 including data rocket motor slag with explosive and collision fragments. It is apparent that there is a strong directional component to the flux in terms of the impact azimuth distribution (Fig. 10(a)) and also the impact velocity (Fig. 10(b)). The majority of impacts are due to the significant debris present on sun-synchronised orbits at inclination near 90° . The ISS which orbits at 52° is impacted by this flux at most angles except in the forward direction at 0° . Both the impact flux and debris velocity peak near $\pm 50^\circ$ and diminish at large angles towards the backward directions.

We can consider the two types of operational modes, those are backward and forward modes. As can be seen in Fig. 10(b), the velocities of the debris relative to ISS are as low as, or less than 2 km s^{-1} in the backward direction ($180^\circ \pm 15^\circ$). In this case, there are less demands for rapid tracking and beam steering, and thus complete removal of all the debris in the range is possible by an operation with one encounter (Eq. (15) and Fig. 9). On the other hand, just a dozen operations are expected in one year (Table 1), since the flux from backward is as low as $10^{-7} \text{ m}^{-2} \text{ yr}^{-1}$.

The situation is different in the case near the forward direction ($50^\circ \pm 15^\circ$ for example). The relative velocity from the forward direction is higher ($\sim 10 \text{ km s}^{-1}$) so that the complete removal of the debris smaller than 6 cm is possible (Eq. (15) and Fig. 9). Here, the flux from the forward direction is also increased to $2 \times 10^{-6} \text{ m}^{-2} \text{ yr}^{-1}$ and more than 200 debris will be detected and treated. Compared to the total flux distribution, Fig. 10(c), with the

directional components, Fig. 10(d), it is clear that the relative forward direction debris is the dominating component by almost 2 orders of magnitude.

Using the pointing configuration shown in Fig. 6, we can calculate the amount of orbit reduction (Δr) possible for different debris sizes from 5 mm to 10 cm. As shown in Fig. 11 using Eq. (15). Here two orbits are considered, that of the ISS where prototype systems would be demonstrated and that near 800 km for a dedicated orbiting system which will be discussed in next section.

4.3. Free orbiting system

If such a remediation solution from the environs of the ISS is successfully demonstrated, one should think of a mission fully dedicated to the debris removal at critical orbits near 800 km altitude where there are many more satellites and indeed greater abundance of debris (flux $\times 10$) as shown in Fig. 1(b). The strategy of the removal operation must be carefully built-up based on the debris distribution in the position-velocity phase space. Such a system would be the ultimate goal after the proof of concept demonstration on the ISS.

Fig. 12(a) 2D flux of debris is plotted against the azimuthal angle from the motion of the direction at the polar orbit at the altitude of 800 km. (b) The relative velocity of debris from the backward direction (azimuth $\sim 100\text{--}180^\circ$) is plotted against the azimuth angle from the direction of motion. Colours represent the 2-D flux of the debris with the size of 0.5–10 cm. (c) The size distribution of the debris at 800 km altitude, the size distribution of debris in ISS orbit. (d) Debris distribution at the ISS orbit from backward ($180 \pm 15^\circ$) and forward ($0 \pm 15^\circ$) direction.

A useful comparison here is with L'ADROIT system proposed by Phipps [4]. Here a novel double mirror catadioptric system, developed by Köse and Perline [17], is implemented to provide the super-wide angle ($\pm 30^\circ$) passive detector. Active tracking and impulse control is provided by a 1.5 m Cassegrain system coupled to a powerful laser system

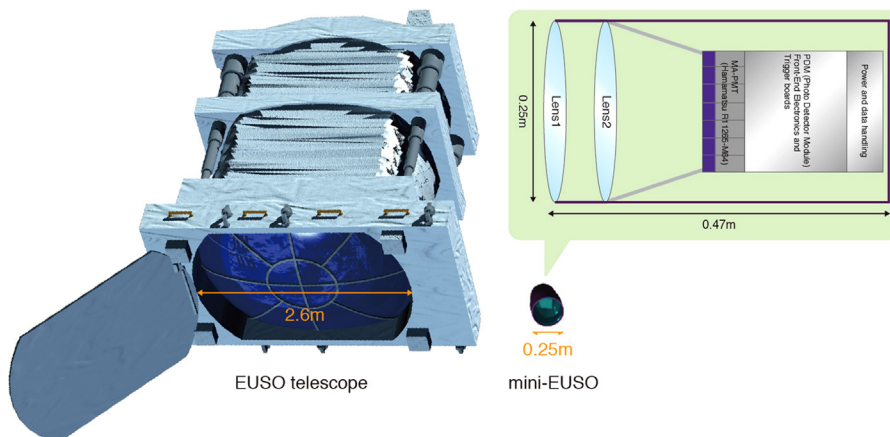


Fig. 9. The comparison of the EUSO telescope with its prototype mini-EUSO.

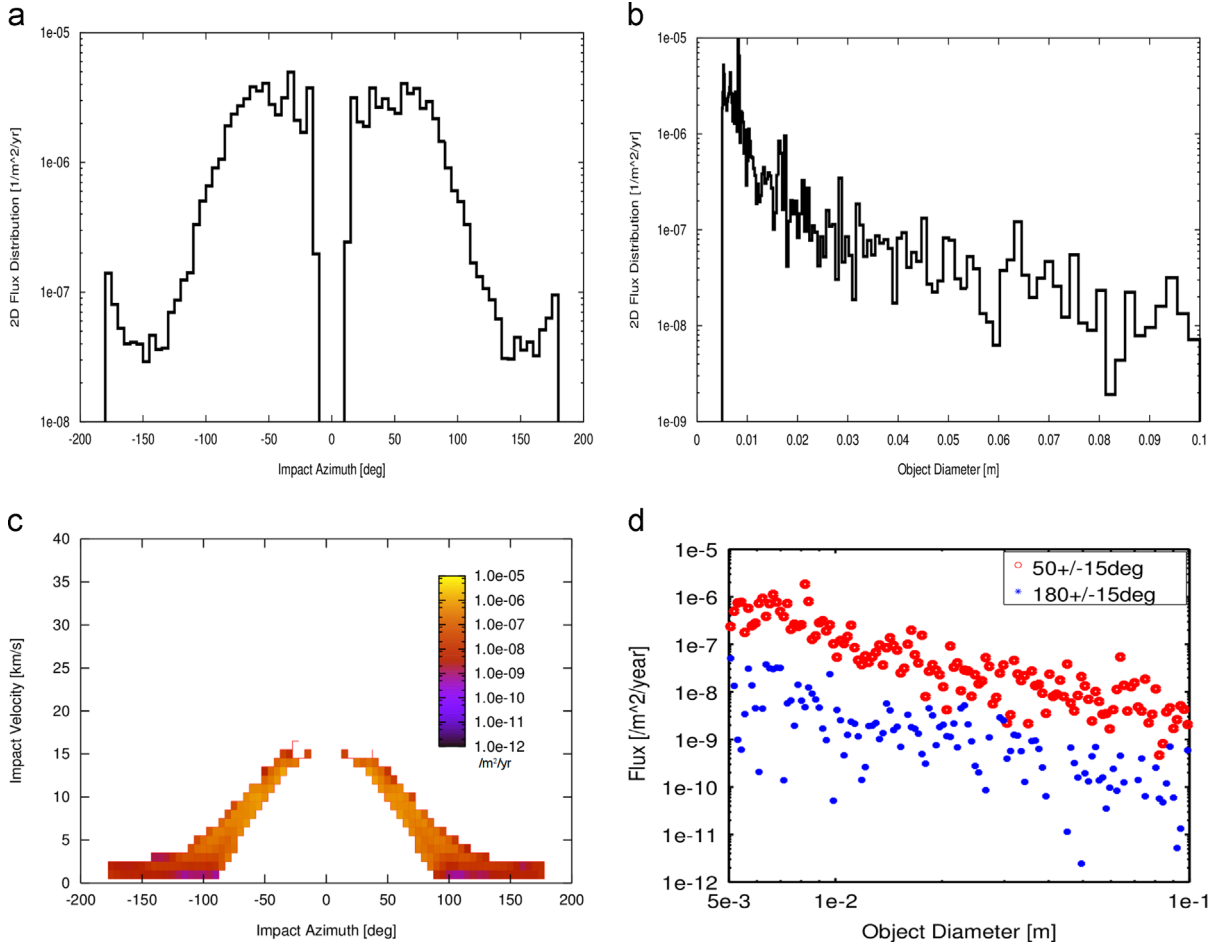


Fig. 10. (a) Distribution of debris in azimuth-velocity diagram at the ISS orbit. The flux for forward direction (azimuth ~ 0) is higher because of the larger relative velocity than that of the backward direction (azimuth $\sim 180^\circ$). (b) The relative velocity of debris from the backward direction (azimuth $\sim 100\text{--}180^\circ$) is plotted against the azimuth angle from the direction of motion. It is as low as 2 km s^{-1} from the backward direction. Colours represent the 2D flux of the debris with the size of 0.5 cm to 10 cm. (c) The size distribution of debris in ISS orbit. (d) Debris distribution at the ISS orbit from backward ($180 \pm 15^\circ$) and forward ($50 \pm 15^\circ$) direction.

producing 100 ps pulses of UV energy ($> 188\text{ J}$) at $< 20\text{ Hz}$ repetition. Phipps also specifies an elliptical polar orbit ranging from 560 km perigee to 960 km apogee.

Analysis of this orbit for 5 mm to 10 cm debris is shown in Fig. 12. The total flux here is $9 \times 10^{-3}\text{ m}^{-1}\text{ yr}^{-1}$ which is a factor of 10 greater than for the ISS orbit. Impact angle is peaked in the forward direction (Fig. 12(a)) and therefore impulse interaction with these debris will involve relative velocities of 15 km s^{-1} as shown in Fig. 12(b). This forward flux is increased by an order of magnitude compared to the ISS orbit while the backwards direction is relatively unchanged as shown in Fig. 12(d).

Operating a free orbiting system to remediate this debris, we propose a functionally similar system to that of Phipps but much more feasible from the technical point of view. As summarised in Table 1, our system consists of an EUSO telescope with a diameter of 2.5 m for debris detection and an 1.5 m Casegrain optics connecting to highly parallel ($> 10^4$) CAN laser system for debris manoeuvre. Both of them have certain technical basis ready to use in ground. Only thing that we have to do is the

increase in repetition rate up to five times than the technical demonstrator on-board ISS. It has an ability to reduce altitudes of the most of debris less than 0.1 m by 500 km by one encounter with the relative velocity of $2\text{--}17\text{ km s}^{-1}$ at the altitude near 800 km (Fig. 12). If we adopt a larger tilt angle of EUSO and tracking/shooting optics towards almost 90° , the performance in orbital reduction could increase still, because of a smaller angle between the debris velocity and reaction force by laser ablation.

Since the debris flux is as high as $\sim 10^{-4}\text{ m}^{-2}\text{ yr}^{-1}$ (Fig. 11) and the cross section of the operation area is $1.6 \times 10^9\text{ m}^2$ (Eq. (17)), the system can operate against 1.0×10^5 debris per year (one per five minutes): the dedicated system is oriented above the horizon to be functional in whole the daytime. Since the polar orbit crosses all the possible orbits at the same altitude, the sweep-up time for a target zone of thickness $\Delta h = 70\text{ km}$ around the system is estimated by [13]

$$\tau_{sw} = \frac{4\pi r^2 \Delta h}{v \Omega A_{sh}}$$

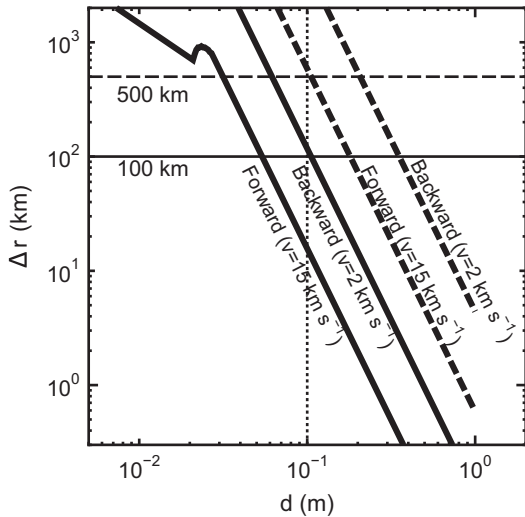


Fig. 11. Reduction in orbital radius are plotted against the debris size d by the technical demonstrator on-board ISS (Solid lines; $\theta_1 = 40^\circ$ and $\theta_2 = 10^\circ$, and $R = 10^4$) for the cases of backward ($v = 2 \text{ km s}^{-1}$) and forward ($v = 15 \text{ km s}^{-1}$). Those by a laser operation of the dedicated laser removal system located at the latitude of 800–900 km (dashed lines; $\theta_1 = 40^\circ$ and $\theta_2 = 10^\circ$, and $R = 5 \times 10^4$), described in Section 2.3.

$$= 2.0 \times 10^6 \left(\frac{r}{7200 \text{ km}} \right)^2 \left(\frac{\Delta h}{70 \text{ km}} \right) \left(\frac{v}{17 \text{ km s}^{-1}} \right)^{-1} \times \left(\frac{\Omega}{0.82 \text{ str}} \right)^{-1} \left(\frac{A_{\text{sh}}}{1.6 \times 10^9 \text{ m}^2} \right)^{-1} s, \quad (19)$$

The system may start from the orbit of an altitude of 1000 km and gradually reduce its orbit in the rate of 10 km per month. After 50 months (~ 4 years), it reaches 500 km removing most of the cm size debris between from 1000 km to 500 km.

5. Discussions and conclusions

Increasing numbers of debris at higher orbits are elevating the risk of future collisions to both functional and derelict satellites. Remediation of cm-size debris which poses the main threat would require directed impulse control to promote atmospheric re-entry. Development of an orbiting debris sweeper, such as that described in recent articles, should be presided by a staged implementation of the novel technologies. We believe that the ISS can provide such an environment enabling scaling and rigorous testing of individual subsystems such as power, detection and laser impulse delivery.

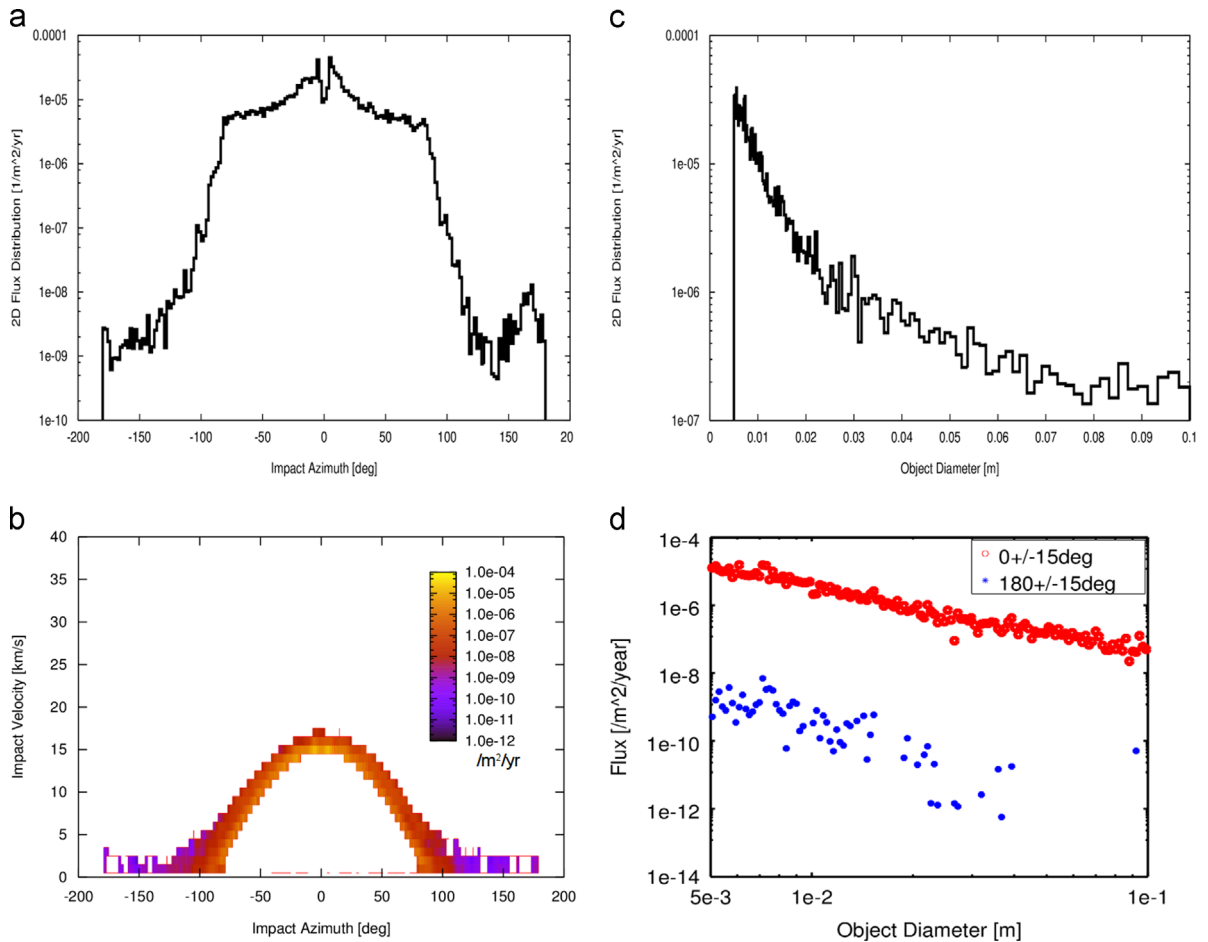


Fig. 12. (a) 2D flux of debris is plotted against the azimuthal angle from the motion of the direction at the polar orbit at the altitude of 800 km. (b) The relative velocity of debris from the backward direction (azimuth ~ 100 – 180°) is plotted against the azimuth angle from the direction of motion. Colours represent the 2-D flux of the debris with the size of 0.5 cm to 10 cm. (c) The size distribution of the debris at 800 km altitude, the size distribution of debris in ISS orbit. (d) Debris distribution at the ISS orbit from backward ($180 \pm 15^\circ$) and forward ($0 \pm 15^\circ$) direction. (For interpretation of the references to colour in this figure legend, the reader is referred to the web version of this article.)

Utilisation of the EUSO telescope on-board the ISS can be accomplished without significant changes to the existing design as a proof of principle wide angle detector of debris. Originally configured for nadir operation with provision to tilt astern to the direction of the motion by $\approx 25^\circ$, this system would provide passive detection of cm scale debris at ranges > 100 km, from the ISS orbit. Measured population data for such small debris would greatly complement the computation models used to predict risks to orbital payloads. No major obstacles are foreseen in implementing a debris detection mode to the operation of this orbiting air-shower telescope. In orbit, a robust, electrically efficient laser system such as that built on the CAN architecture would be required. Attributes of stability and good beam quality would enable precise taking and impulse delivery from distances > 100 km.

Laser impulse control can also be used to modify the rotation rate of large debris objects such as derelict satellites or spent rockets. Prior to their capture by dedicated removal spacecraft it is necessary to stop their rotation. The moment of impact necessary to stop the rotation is in the order of 10^2 N s m for the case of a typical satellite with the mass of 1000 kg the size of 1 m, and angular velocity of 0.1 Hz. It takes only several minutes to give this amount of impulse using a 1 kW laser system. Also the precise orbital injection of a satellite can be done remotely with 10 kW-class space laser system without additional propellant in the satellite. It may give us a significant freedom for the operation of the orbital bodies.

In conclusion, we have proposed a staged approach to the development of a space based system for the remediation of orbital debris fragments from 5 mm to 10 cm in size. Beginning with demonstration missions on the International Space Station incorporating the EUSO module as a detector, we have shown that there are sufficient debris numbers to validate proof-of-principle operation of both tracking and remediation capability with the efficient fibre-based CAN laser system. This would lay the ground-work for a freely orbiting system to carry our remediation at higher altitudes where debris risks are increasing for highly populated polar orbits where $> 10^4$ debris fragments would be removed per year.

Acknowledgement

This work was partially supported by JSPS KAKENHI Nos. 23340081, 24244042, and RIKEN Strategic Research Programs for R&D in Japan, the CEA, l'Ecole Polytechnique and Thales in France.

References

- [1] Liou, J.-C., & Krisko, P., N update on the effectiveness of postmission disposal in leo, in: Proceedings of the 64th International Astronautical Congress, IAC-13-A6.4.2, Beijing, China, 2013.
- [2] S. Flegel, et al., MASTER2009, Technische Universitt Braunschweig, Institute of Aerospace Systems, 2011 Final report.
- [3] J.D. Metzger, et al., J. Propuls. Power 5 (1989) 582–590.
- [4] C.R. Phipps, L'ADROIT – A spaceborne ultraviolet laser system for space debris clearing, ActaAstronaut. 104 (2014) 243–255.
- [5] W.O. Schall, Laser requirements for the removal of space debris from orbit, Proc. SPIE 3574 (1998) 426–436.
- [6] D.A. Liedahl, A. Rubenchik, S.B. Libby, et al., Pulsed laser interactions with space debris: target shape effects, Adv. Space Res. 52 (5) (2013) 895–915, <http://dx.doi.org/10.1016/j.asr.2013.05.019>.
- [7] Y. Takahashi, et al., The JEM-EUSO mission, New J. Phys. 11 (2008) 065009.
- [8] M. Casolino, J.H. Adams, M.E. Bertaina, et al., Detecting ultra-high energy cosmic rays from space with unprecedented acceptance: objectives and design of the JEM-EUSO mission, Astrophys. Space Sci. Trans. 7 (2011) 477.
- [9] R. Soulard, et al., A novel laser architecture for space debris removal, Acta. Astronaut. 105 (2014) 192–200.
- [10] J.H. Adams Jr., An evaluation of the exposure in nadir observation of the JEM-EUSO mission, Astropart. Phys. 44 (2013) 76–90.
- [11] C.W. Allen, Astrophysical Quantities, third ed. University of London, Athlone Press Ltd., London, 1973.
- [12] C. Phipps, et al., Laser impulse coupling at 130 fs, Appl. Surf. Sci. 252 (2006) 4838–4844.
- [13] G. Mourou, et al., The future is fibre accelerators, Nat. Photonics 7 (2013) 258–261.
- [14] J. Bourderionnet, C. Bellanger, J. Primot, A. Brignon, Collective coherent phase combining of 64 fibres, Opt. Express 19 (2011) 18.
- [15] A. Klenke, S. Breikopf, M. Kienel, 530 W, 1.3 mJ, four-channel coherently combined femtosecond fiber chirped-pulse amplification system, Opt. Lett. 38 (2013) 2283–2285.
- [16] Bourderionnet, J., et al. Continuous laser beam steering with micro-optical arrays: experimental results, in: Proceedings of the SPIE Europe Security and Defence, International Society for Optics and Photonics, 2008.
- [17] E. Köse, R.K. Perline, Double-mirror catadioptric sensors with ultra-wide field of view and no distortion, Appl. Opt. 53 (2014) 528–536.